Numerical Investigation of Whistling Noise from Vehicle Side Mirrors

Xing Peng[1], Jiang Zuxiao[1,2,3], Chen Shengxian[2]

1. Shanghai Ground Vehicle Wind Tunnel Center, Tongji University, No. 4800, Caoan Highway, Jiading District, Shanghai;

2. Product Development Department, SAIC Volkswagen Automotive Co., Ltd., No. 63, Luopu Road, Jiading District, Shanghai;

3. Tongji University School of Automotive Studies, Tongji University, No. 4800, Caoan Highway, Jiading District, Shanghai

xingpeng@tongji.edu.cn

jiangzuxiao@csvw.com

chenshengxian@csvw.com

Abstract: Under specific driving conditions, the airflow passing through the vehicle's side mirrors can generate high-frequency noise with narrowband frequency characteristics, commonly referred to as whistling. The causes of whistling are multifaceted and include factors such as gaps, shape, and periodic airflow motion. Different mechanisms of whistling generation necessitate distinct solutions. In this paper, whistling was detected during subjective evaluation in the wind tunnel. Through wind tunnel testing and acoustic array analysis, the frequency of the whistling was identified, and the airflow velocity and yaw angle were determined. Subsequently, numerical analysis of the wall-bounded airflow near the side mirrors was conducted using a transitional transport function incorporating intermittency and momentum thickness Reynolds number corrections. The analysis revealed that the separation and reattachment of the laminar boundary layer led to localized turbulence enhancement, which was identified as the cause of whistling. Based on these findings, two optimization schemes for promoting early transition of the laminar flow were proposed and validated through simulations. The simulation results demonstrated that designs incorporating steps or modifications to surface roughness could effectively

Contribution: 2025 FKFS Conference on Vehicle Aerodynamics and Thermal Management
15 – 16 October 2025 | Leinfelden-Echterdingen

prevent the separation of the laminar boundary layer, thereby eliminating the generation of whistling. Moreover, the simulation results were found to be consistent with the experimental findings. This study not only elucidated the mechanism of whistling generation due to the shape of the side mirrors but also provided a theoretical basis and technical support for the design optimization of vehicle side mirrors.

1 Intruduction

As a complex mechanical system, a vehicle generates noise from multiple sources. While traditional automotive noise arises from the powertrain, tires, and aerodynamic effects, wind noise has become increasingly dominant, particularly with the growing use of high-speed urban roads and electric vehicles. The absence of engine noise in electric vehicles further amplifies the perception of wind-induced sound, making aerodynamic noise control a critical factor in enhancing in-cabin sound quality. Wind noise control typically involves three main strategies: leakage sealing, acoustic package design, and aerodynamic shape optimization. Leakage control focuses on sealing elements like glass and door seals; acoustic packages address broadband insulation, especially across firewall and floor panels. In contrast, aerodynamic shape design targets unsteady flow phenomena around exterior features-most notably the A-pillar and rearview mirror, which are known contributors to wind noise. Among these, the rearview mirror is particularly sensitive due to its protruding geometry. Unlike sealing and acoustic strategies, mirror-induced whistling noise lacks a well-established theoretical framework. Whistling is often triggered by shear flow instabilities when the flow reaches a critical velocity. Chanaud[1] classified flow-induced feedback mechanisms into three types: Type I involves purely hydrodynamic feedback from vortex shedding; Type II includes near-field acoustic feedback; and Type III covers far-field acoustic feedback, such as cavity resonance. Rearview mirror whistling is generally associated with Type II or III, due to its coupling of flow and sound. Although aerodynamic noise has been widely studied, mirror-specific whistling research remains limited. Prior works have examined general flow instabilities. Hucho[2] discussed some fundamental mechanisms of fluid, but this is usually limited to the development of laminar and turbulent boundary layers on flat plates or general shapes (airfoils or cylinders). Lucas[3] believes that the basic excitation mechanisms of whistling are mainly divided into mixing layers, jets, wakes, vortices, and cavities. Yang[4] analyzed the feedback mechanism and considered that the characteristic steps of feedback are the process of vortex generation, vortex shedding, aerodynamic noise generation, vortex regeneration, re-shedding, and aerodynamic noise regeneration. Vaik[5-6] studied an edge-tone configuration, which consists of a planar free jet impinging on a wedge-shaped object. They conducted a

parametric study on the velocity profiles of different types of jets by changing the average exit velocity of the jet and the distance from the nozzle to the wedge configuration, and proposed a set of formulas for predicting the frequency of edge tones. Sun[7] investigated the flow instability of a two-dimensional open cavity by varying the free-stream Mach number from 0.1 to 1.6 and provided stability curves over a wide range of Mach and Reynolds numbers. Yamouni[8] conducted a global stability analysis of open cavities, explaining that under incompressible conditions (Ma<0.3), the flow is affected by global instabilities due to the Kelvin-Helmholtz effect in the shear layer and, this instability is intensified by fluid dynamic pressure feedback. Under compressible conditions, as the Mach number decreases, all unstable global modes gradually transition to incompressible (Ma>0.3) shear layer modes. Lounsberry[9] experimentally studied the fluid changes in the laminar separation region on the rearview mirror housing. The boundary layer starts as laminar and then transitions to turbulent, and attempts were made to induce turbulence in the boundary layer early to eliminate whistling. Huang Lina[10] used the oil flow method in wind tunnel tests to observe the flow state on the vehicle's longitudinal symmetry plane and the side window position of the rearview mirror, but did not observe and analyze the flow phenomena on the surface of the rearview mirror. Guan Peng et al.[11] analyzed and optimized whistling and broadband noise through a combination of simulation and experiments, but did not find a specific method for analyzing rearview mirror whistling. Jiang Zuxiao et al.[12] measured the aerodynamic noise characteristics in the rearview mirror wake region through wind tunnel tests, analyzed the noise performance of the rearview mirror at different vehicle speeds, and solved the rearview mirror whistling problem through experimental research. Wu Haibo et al.[13] used a new transition model to simulate the fluid changes in the laminar boundary layer on the rearview mirror surface and validated the effectiveness of the method through wind tunnel tests. However, none of the above studies have provided a comprehensive explanation of the rearview mirror shape whistling problem.

In this study, wind tunnel experiments on a clay prototype vehicle revealed a whistling phenomenon at specific flow speeds and yaw angles. Acoustic arrays were used to localize the sound source and identify its narrowband frequency. The cause was traced to geometric features of the rearview mirror. A numerical simulation using the Local Correlation-based Transition Model (LCTM) was conducted to analyze shear stress, momentum thickness, and turbulent kinetic energy near the mirror surface. The results showed that laminar boundary layer separation and reattachment led to localized turbulence amplification, which triggered the whistling. Based on the findings, two design strategies-introducing a step and modifying surface roughness-were proposed to promote early transition and prevent separation. Wind tunnel validation confirmed the effectiveness of these solutions, providing practical guidance for the aerodynamic design of noise-optimized rearview mirror.

2 Problem identification and diagnosis

2.1 Problem identification

2.1.1 Test facility

The experimental tests were conducted at the Full-Scale Aeroacoustic Wind Tunnel of the Shanghai Ground Transportation Wind Tunnel Center, Tongji University. This facility is a 3/4 open-return wind tunnel with three open sides at the nozzle and one side connected to the ground. During testing, the prototype vehicle was fixed at the center of the turntable located on the wind tunnel balance platform. For this study, both the boundary layer suction system and the moving ground belt were deactivated during operation, as per standard acoustic testing protocols[14].

2.1.2 Subjective and Objective Evaluation

The evaluation was divided into two parts: subjective assessment and objective testing. Subjective evaluation focused on the overall perception of the external acoustic field in the wind tunnel under different speeds and yaw angles. Objective testing included external field measurements and acoustic imaging to verify the presence and characteristics of aerodynamic noise.

Based on the known generation and propagation mechanisms of aerodynamic noise, the tests considered the following key factors:

(1) Aerodynamic noise becomes dominant at high speeds, typically above 100 km/h.

(2) Crosswind conditions not only affect driving stability but also significantly influence wind noise characteristics. Therefore, yaw angles were introduced during the tests.

Accordingly, the subjective evaluation was conducted at speeds between 100 km/h and 140 km/h and yaw angles of ±5° and ±10°. During evaluation, a distinct whistling noise was audibly detected on the right-hand side of the vehicle exterior when the yaw angle was -5° and the wind speed approached 125 km/h.

To confirm the existence of the whistling noise, objective testing was conducted. The center of the balance turntable was defined as the origin (0, 0, 0), with a diameter of 11 m. The X-axis pointed from the nozzle toward the collector, while the Y-axis was perpendicular to it. Two free-field microphones were placed symmetrically at a height of 1.2 m from the ground, located at coordinates (0, ±6 m, 1.2 m), as illustrated in Figure 1.

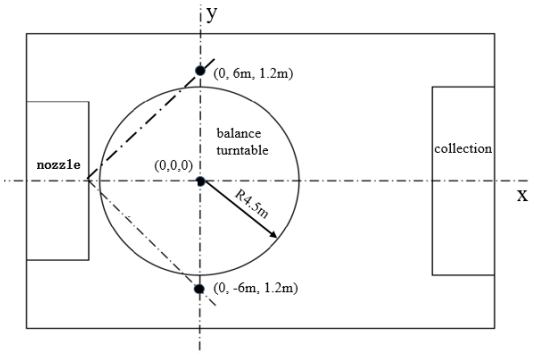

Figure 1: Schematic diagram of the test setup

The data acquisition period was 10 seconds, and the frequency range for noise analysis was 500–10,000 Hz. The FFT results are shown in Figure2.

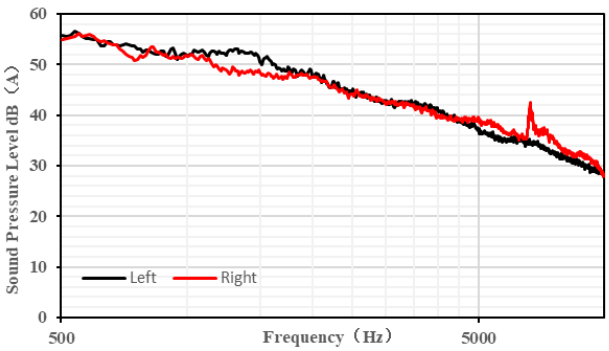

Figure 2: SPL results from external flow-field microphones

As shown in Figure 2, the sound pressure level (SPL) on the vehicle's right-hand side generally decreases with increasing frequency. However, a narrowband peak is observed at 6668 Hz, where the right-side SPL is 8.3 dB(A) higher than the left side. This result aligns with the subjective evaluation, confirming the presence of a whistling noise originating from the vehicle's right-side exterior flow field.

2.2 Diagnostic Process

Whistling noise can originate from various aerodynamic sources, including gap-induced whistling, geometry-induced resonance, and periodic flow instabilities. To identify the precise source and location of the noise, multiple experimental techniques were employed within the wind tunnel.

2.2.1 Acoustic Array Testing

An acoustic array is a visual-acoustic measurement system composed of multiple synchronized microphones, as illustrated in Figure 3. It can generate acoustic images or animations to help localize and characterize noise sources. In this study, a 120-channel spiral microphone array was positioned on the right-hand side of the test vehicle, carefully placed outside the influence of high-speed airflow.

Targeted acoustic imaging and scanning were performed for key regions including the front grille, front wheels, and rearview mirror. The objective was to identify the spatial distribution of aerodynamic noise across these areas.

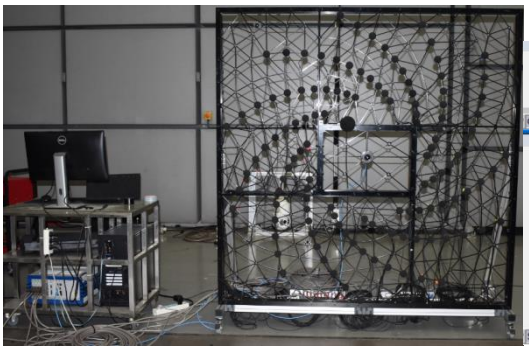

Figure 3: Acoustic array test setup

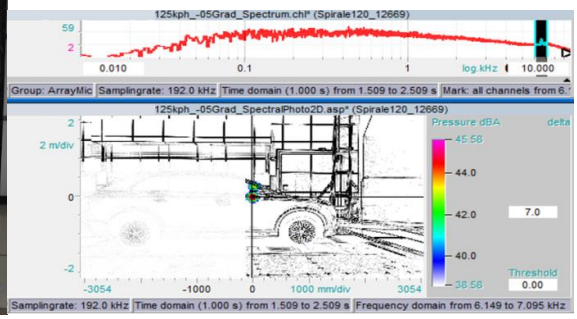

Figure 4: Acoustic imaging result from microphone array

The measurement results from the acoustic array are shown in Figure 4. A clear tonal peak was observed in the frequency band between 6149 Hz and 7095 Hz, consistent with the previously identified peak at 6668 Hz from the external field SPL measurements. These findings strongly confirm that the whistling noise originates from the rearview mirror region.

2.2.2 Source Confirmation of Whistling Noise

Following the acoustic array localization, the rearview mirror was confirmed as the origin of the whistling noise. However, the exact noise generation mechanism remained unclear. Based on structural analysis, two possible mechanisms were hypothesized: gap-induced whistling and geometry-induced resonance. To eliminate the first possibility, all gaps on the mirror surface were sealed with adhesive tape to block airflow entering internal cavities. After sealing, the whistling noise persisted during testing. Therefore, the source was attributed to an unfavorable surface geometry, suggesting that the noise was primarily caused by geometry-induced whistling.

3 Analysis of Underlying Mechanism

3.1 Linear Stability Theory

Boundary layer disturbances are inherently complex, and the transition from laminar to turbulent flow remains a key topic in fluid dynamics. Among various predictive models, linear stability theory (LST) is one of the most widely used. LST assumes that disturbances superimpose linearly on a steady base flow and that their amplitudes are sufficiently small not to affect the mean flow. Under this framework, the flow can be decomposed into a base state and small-amplitude perturbations, often expressed as temporal or spatial waves. By examining the growth rate of these disturbances, LST provides a theoretical means to predict flow instability onset conditions[15].

Although LST cannot fully describe the physical mechanisms of transition or predict nonlinear developments, it remains a powerful tool in understanding early-stage instability and guiding flow control strategies. It has also helped researchers analyze natural and bypass transition processes by capturing the evolution of Tollmien–Schlichting (T-S) waves and their interaction with vortical structures[16].

3.2 Tollmien–Schlichting (T-S) Waves

According to Chanaud's classification of whistling mechanisms, the rearview mirror noise can be attributed to a Type II feedback loop. This involves laminar boundary layer instabilities triggered by external disturbances, which manifest initially as two-dimensional T-S waves. These waves propagate along the surface, gradually evolving into three-dimensional structures, inducing low-amplitude pressure fluctuations while the flow remains nominally laminar.

As disturbances amplify, secondary instabilities emerge, generating turbulent patches and localized noise radiation. Part of the acoustic energy feeds back into the upstream flow, promoting earlier transition to turbulence near the mirror front. The resulting turbulence further energizes the feedback loop, forming a self-sustained T-S cycle that leads to discrete tonal peaks in the sound spectrum—characteristic of aerodynamic whistling consistent with Type II resonance.

This phenomenon, first hypothesized by Prandtl and later formalized by Tollmien and Schlichting[17], forms a natural instability pathway in low-turbulence environments. In particular, laminar separation bubbles provide a fertile ground for T-S wave amplification, with separation and reattachment enhancing the flow's receptivity to acoustic excitation. Such feedback between unstable shear layers and surface

geometry drives the sustained tonal noise observed in this study.

The interaction between weak acoustic perturbations and transitional shear layers not only underscores the sensitivity of the boundary layer to external forcing but also demonstrates how seemingly minor acoustic energy can reinforce turbulence. This feedback loop offers critical insight into the physical mechanism behind mirror-induced whistling and supports the use of T-S wave theory in aerodynamic noise diagnostics.

4 Numerical Analysis

In aerodynamics, transition is typically the result of flow instability, where small disturbances grow exponentially and ultimately trigger nonlinear breakdown into turbulence. One key mechanism is separation-induced transition, in which a laminar boundary layer separates under an adverse pressure gradient. Transition then develops within the detached shear layer, and the now-turbulent boundary layer may reattach under a strong favorable pressure gradient.

In this study, a transition model based on turbulence modeling was applied—specifically, the Local Correlation-based Transition Model (LCTM). The LCTM is a transport-equation-based model that relies exclusively on local flow variables, enabling efficient and practical integration into Reynolds-Averaged Navier–Stokes (RANS) simulations. It is particularly well-suited for predicting transitional flows where laminar regions exist within a predominantly turbulent boundary layer, as is common in aerodynamic whistling problems.

4.1 $\gamma - Re_\theta$ Transition Model

The LCTM adopted in this study is based on the two-equation correlation-based transition model developed by Menter et al[18-19]. This hybrid model retains the original turbulence model formulation near the wall and modifies it in the outer boundary layer to account for transition onset and progression. The governing transport equations for intermittency (γ) are expressed as:

$$\frac{\partial(\rho\kappa)}{\partial t} + \nabla\cdot(\rho U\kappa) = \nabla\cdot\left(\left(\mu + \frac{\mu_t}{\sigma_\kappa}\right)\nabla\kappa\right) + P_\kappa - D_\kappa \qquad (1)$$

$$\frac{\partial(\rho\omega)}{\partial t} + \nabla\cdot(\rho U\omega) = \nabla\cdot\left(\left(\mu + \frac{\mu_t}{\sigma_\kappa}\right)\nabla\omega\right) + \frac{\gamma}{v_t}P_\kappa - \beta\rho\omega^2 + \ldots$$

$$+2(1-F_1)\frac{\rho\sigma\omega_2}{\omega}\nabla\kappa:\nabla\omega \quad (2)$$

The terms, P_κ and D_κ in the model represent the production and dissipation of turbulent kinetic energy. ρ denotes the fluid density. U is the velocity field. μ_t is the turbulent viscosity. ω is the specific dissipation rate of turbulence.

The baseline turbulence model is inherently suitable for fully turbulent boundary layers. However, to accurately simulate laminar boundary layers and transitional regions, modifications to the production and dissipation terms of turbulent kinetic energy are required. For this purpose, a variable known as turbulence intermittency (γ) is introduced, which represents the time-averaged fraction of turbulent fluctuations within the boundary layer.

$$\frac{\partial(\rho\gamma)}{\partial t}+\nabla\cdot(\rho U\gamma)=\nabla\cdot\left(\left(\mu+\frac{\mu_t}{\sigma_\gamma}\right)\nabla\gamma\right)+P_\gamma-D_\gamma \quad (3)$$

$$\frac{\partial(\rho\omega)}{\partial t}+\nabla\cdot(\rho U\omega)=\nabla\cdot\left(\left(\mu+\frac{\mu_t}{\sigma_\kappa}\right)\nabla\omega\right)+\frac{\gamma}{v_t}P_\kappa-\beta\rho\omega^2+2(1-F_1)\frac{\rho\sigma\omega_2}{\omega}\nabla\kappa:\nabla\omega(2)$$

The terms , P_κ and D_κ in the model represent the production and dissipation of turbulent kinetic energy. ρ denotes the fluid density. U is the velocity field. μ_t is the turbulent viscosity. ω is the specific dissipation rate of turbulence.

The baseline turbulence model is inherently suitable for fully turbulent boundary layers. However, to accurately simulate laminar boundary layers and transitional regions, modifications tu the production and dissipation terms of turbulent kinetic energy are required. For this purpose, a variable known as turbulence intermittency (γ) is introduced, which represents the time-averaged fraction of turbulent fluctuations within the boundary layer. Thr transport equation for intermittency is expressed as:

$$\frac{\partial(\rho\gamma)}{\partial t}+\nabla\cdot(\rho U\gamma)=\nabla\cdot\left(\left(\mu+\frac{\mu_t}{\sigma_\gamma}\right)\nabla\gamma\right)+P_\gamma-D_\gamma \quad (3)$$

The production term of turbulence intermittency γ governs the length and onset of the transition region P_γ. It is defined as:

$$P_\gamma=F_{length}c_{\alpha1}\rho S(\gamma F_{onset})^{0.5}(1-c_{e1}\gamma) \quad (4)$$

Here, S is the local strain rate magnitude. F_{length} is a non-dimensional function controlling the length of the transition region. F_{onset} is another non-dimensional function used to control the onset location of transition. Both of them are non-dimensional functions used to control the intermittency transport equation within the boundary layer. They modulate the growth and onset of intermittency based on local

flow conditions. The destruction or relaminarization source term in the intermittency equation is defined as:

$$D_\gamma = c_{\alpha 2}\rho\Omega\Upsilon F_{turb}(c_{e2}\gamma - 1) \quad (5)$$

Here, Ω represents the vorticity magnitude, which serves to prevent the destruction of intermittency in the freestream caused by high strain rates. The model constant: $c_{\alpha 1} = 2.0,\ c_{\alpha 2} = 0.06$, It controls the strength of the destruction term and ensures that the entire term remains less than the turbulent Prandtl number $c_{e1} = 1.0,\ c_{e2} = 50.0$. It sets the lower bound of intermittency, and a threshold value of 50 is sufficiently low to preserve laminar flow in the boundary layer. F_{turb}It is used to deactivate the destruction term in fully turbulent regions[18].

4.2 Numerical Simulation Model

To reproduce the whistling caused by the rearview mirror geometry, a simplified vehicle model was constructed. Non-critical features such as the front grille, underbody, and minor grooves were sealed to reduce computational cost. Key flow-affecting elements—such as the A-pillar, windshield, and detailed mirror geometry (gaps, steps)—were retained. A half-car model was used based on wind tunnel observations indicating whistling on the right side. The computational domain was defined with the inlet placed 4 car lengths ahead of the front, the outlet 8 car lengths downstream, lateral boundaries 5 car widths from the side, and the top boundary 8 car heights above the roof. The setup is shown in Figure 5, and boundary conditions are listed in Table 1. According to wind tunnel data, the inlet velocity was set to 125 km/h, and the outlet pressure was set to 0 Pa.

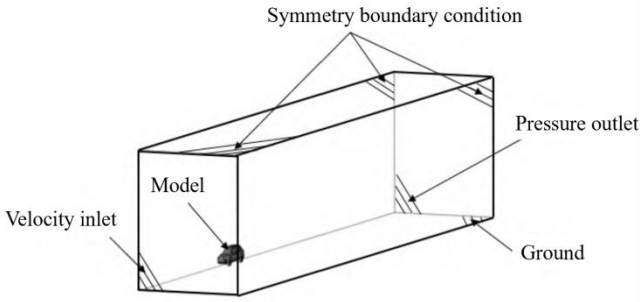

Figure 5. Computational domain of the numerical simulation model.

Table 1. Boundary conditions of the numerical simulation model.

Boundary	Type	Rematks

Inlet	Velocity inlet	145km/h，non-reflecting
Outlet	Pressure outlet	0 Pa, non-reflecting
Side	Symmetry boundary condition	slide

Table 2 summarizes the numerical discretization schemes used in the simulation.

Table 2. Discretization schemes employed in the CFD simulation.

Equations	Scheme
interpolationSchemes	linear
snGradSchmes	limited corrected 0.33
gradSchemes	cellLmited Gauss linear 1
divSchemes	div(phi, U):bounded Gauss linearUpwindV grad(U)
laplacianSchemes	bounded Gauss upwind Gauss linear limited corrected 0.33

To accurately capture the flow near the rearview mirror, local mesh refinement was applied to critical components including the mirror body, A-pillar, and windshield. Table 3 presents the mesh parameters used. The maximum surface mesh size in the computational domain was set to 512 mm. A total of 12 prism layers were generated near walls to resolve boundary layers, with the first-layer height of 0.01 mm and a growth rate of 1.2.

Table 3. Mesh parameters of the simulation model.

Main parameters			
Rearview mirror	Min_0.25mm Max_0.5mm	Front side window glass	1mm
A/B pillars & rain strips	1mm	Rear window glass	2mm
Windshield	8mm	Remaining areas	20mm

To better capture the whistle-generating flow near the side mirror, the mesh around the mirror was refined with 15 boundary layer layers, starting from a first-layer height of 5e-6 m and a growth rate of 1.3. A local refinement zone of 4 mm was also added near the mirror.

4.3 Flow Field Analysis

Using the LCTM transition model, simulations were conducted under a 125 km/h inlet velocity and a yaw angle of -5 degree, with 5000 steady-state iterations. Flow characteristics near the side mirror were evaluated via wall shear stress, momentum thickness, and turbulent kinetic energy (TKE) to assess the potential for tonal noise generation.

4.3.1 Wall Shear Stress

Figure 8 presents the surface velocity contour around the side mirror. As shown in the red-circled region, there is a notable reversal in wall shear stress direction (from negative to positive), indicating a progressive deceleration of near-wall airflow, potentially down to zero velocity- as further illustrated in the velocity field in Figure 7. This variation in velocity results in a local increase in wall shear stress, suggesting that intermittency in the laminar boundary layer is beginning to rise in this area.

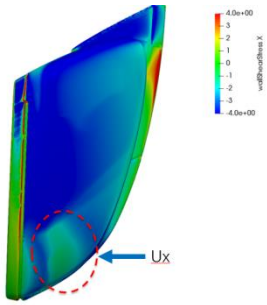

Figure 6. Wall Shear Stress

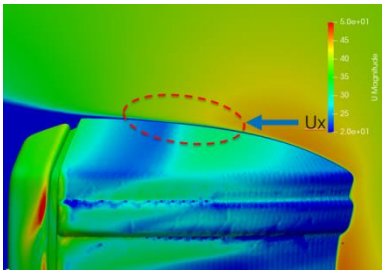

Figure 7. Surface Velocity

4.3.2 Momentum Thickness

As shown in Figure 8, the momentum thickness decreases after initially increasing, indicating a transition from laminar to turbulent boundary layer. The enhanced momentum mixing due to velocity fluctuations in the turbulent layer leads to an increase in momentum thickness. In other words, the variation in momentum thickness reflects the occurrence of boundary layer separation. Momentum thickness is closely related to surface drag. According to the von Kármán integral relation, its rate of change is directly linked to wall shear stress-consistent with the changes observed in shear stress in Figure 6. Furthermore, Figure 7 shows a sequence of thickening followed by thinning of the momentum thickness. This trend confirms that increased momentum loss within the boundary layer causes separation, which significantly raises drag and reduces flow efficiency. When flow velocity drops to zero, momentum thickness reaches its maximum. However, as turbulence intensity and momentum transfer improve, the flow reattaches to the mirror surface. This also suggests that the intermittency criterion within the governing function is no longer satisfied-intermittency gradually returns to zero, deactivating Equation (4), allowing the boundary layer to thin out and re-laminarization.

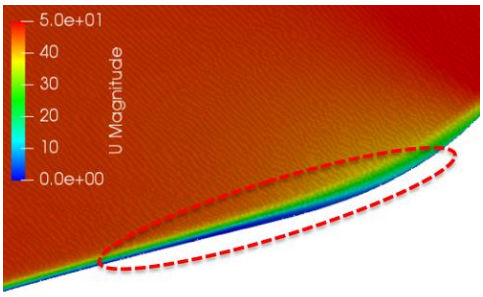

Figure 8. Momentum Thickness

4.3.3 Turbulent Kinetic Energy

TKE influences eddy viscosity and boundary layer stability, directly impacting transition onset and extent. According to Eq. (4), its distribution is critical for transition prediction. The adopted transition model incorporates separation-induced correction terms to better capture TKE evolution near the mirror.

TKE distribution indicates weak turbulence on the mirror surface, suggesting possible transition or laminar separation. The low TKE levels imply the boundary layer remains largely laminar, with instabilities likely triggered by T–S waves. Combined with the momentum thickness variations in Figure 7, the flow is inferred to separate and reattach, enhancing turbulence and pressure fluctuations. This behavior is consistent with the generation of tonal noise and potential acoustic feedback.

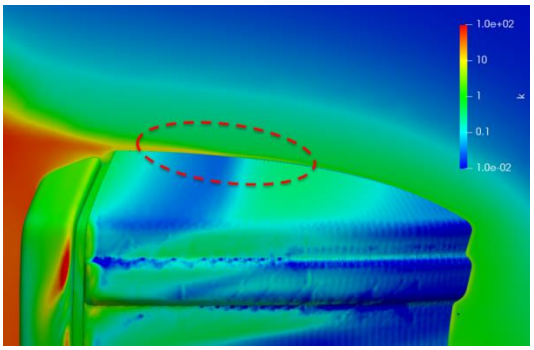

Figure 8. Turbulent Kinetic Energy

5 Optimization

Two mirror modification strategies were proposed to suppress tonal noise: (a) introducing a surface step to trigger early transition, preventing laminar separation; and (b) increasing surface roughness to promote flow attachment and reduce sensitivity to small disturbances. The modified areas are indicated by green lines in Figure 9.

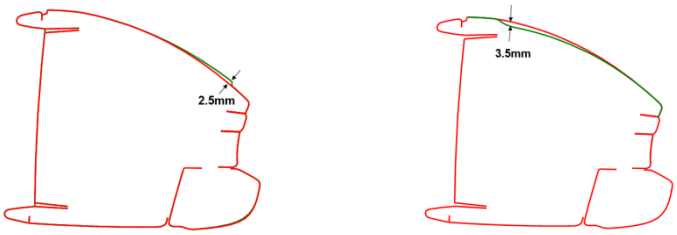

(a) Step Addition Design (b) Rough Surface Design

Figure 9 Modified Mirror Configurations

To verify the effectiveness of both designs, wind tunnel tests were conducted. As shown in Figure 10, neither modified mirror exhibited tonal noise, confirming the suppression of shape-induced whistling.

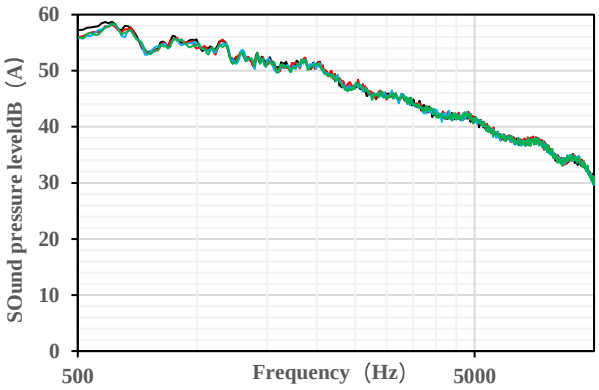

Figure 12 Wind Tunnel Test Results at 140 km/h and -5° Yaw

Based on the previous analysis, numerical simulations were conducted under the test condition of 140 km/h and -5 degree yaw. Flow field results confirmed the role and variation of key parameters during the laminar-to-turbulent transition, offering a predictive approach for early-stage design against tonal noise.

6 Conclusion

This study identified tonal noise issues around the vehicle's side mirror using wind tunnel experiments and investigated the underlying mechanisms via the LCTM transition model. The main conclusions are as follows:

(1) Whistling Identification:

Wind tunnel testing revealed that at 140 km/h and -5degree yaw, the SPL at 6668 Hz was significantly higher than adjacent frequencies, with a peak difference of 8.3 dB(A), confirming the presence of tonal noise on the right side-consistent with subjective evaluation.

(2) Mechanism Determination:

Simulations using the LCTM model analyzed wall shear stress, momentum thickness, and turbulent kinetic energy. Results indicated that the primary cause of mirror-induced tonal noise was laminar boundary layer separation and subsequent reattachment on the mirror surface.

(3) Design Optimization:

Two mirror design optimizations were proposed. Adding a step to promote early laminar-to-turbulent transition. Introducing surface roughness via an L-shaped feature to trigger transition. Both approaches were validated by wind tunnel tests to effectively eliminate tonal noise.

(4) Engineering Implications:

The combined use of simulation and experimental validation effectively resolved the mirror tonal noise issue. This approach is particularly suitable for early-stage vehicle development. Given the diversity of tonal noise types and mechanisms in vehicle design, future work can explore advanced simulation techniques and optimization algorithms to further refine prediction accuracy and coverage.

Reference

[1] Robert C. Chanaud. Aerodynamic whisltes [J]. Scientific American Inc., 1970, 222(1): 40-47.

[2] Thomas Christian Schuetz. Aerodynamics of Road Vehicles [M]. 5th Edition, London, England: SAE International, 2015.

[3] Michael J. Lucas, Robert A Noreen, Louis C Sutherland, et al. Handbook of the acoustic characteristics of turbomachinery cavities [M]. America: Newyork: American society of mechanical engineers, 1997.

[4] Dangguo Yang, Jianqiang Li, Jun Liu, et al. Analysis on physical mechanism of sound generation inside cavities based on acoustic analogy method [J]. Open journal of fluid dynamic, 2013, 3(1): 23-31.

[5] Vaik I, Varga R, Paál G. Frequency and phase characteristics of the edge tone [J]. Part I. Periodica Polytechnica Mechanical Engineering, 2014, 58(1): 55–67. DOI: 10.3311/PPme.7028

[6] Vaik I, Varga R, Paál G. Frequency and phase characteristics of the edge tone [J]. Part II. Periodica Polytechnica Mechanical Engineering, 2014;58(1):69–76. DOI: 10.3311/PPme.7031

[7] Yiyang Sun, Aditya G. Nair, Kunihiko Taira, Louis N. Cattafesta. Numerical simulations of subsonic and transonic open-cavity flows [C]. America: Atlanta: 7th AIAA theoretical fluid mechanics conference, 2014. DOI: http://doi.org/10.2514/6.2014-3092

[8] Sami Yamouni, Denis Sipp, Laurent Jacquin. Interaction between feedback aeroacoustic and acoustic resonance mechanisms in a cavity flow: a global stability analysis [J]. Journal od Fluid Mechanics, 2013, (717): 134-165. DOI: https://doi.org/10.1017/jfm.2012.563

[9] Peter G. Baines, Sharanya Majundar, Humio Mitsudera. The mechanics of the Tollmien-Schlichting wave [J]. Journal of Fluid Mechanics, 1996, (312): 107-124. DOI:10.1017/S0022112096001930

[10] Huang Lina. Research on Unsteady Pressure field and aerodynamic noise [D]. Jinlin University, 2014.

[11] Guan Peng, Pan Lei, Gu Yan. Research on the shape optimization of rear mirror wind noise performance [J]. Automobile applied technology, 2020(11): 113-116. DOI: CNKI:SUN:SXQC.0.2020-11-037

[12] Jiang Zuxiao, Xing Peng, Zhou Jiangbin. Experimental research on whistle characteristics of automobile side mirror [J]. Journal of machine design, 2020, 37(S02): 187-193. DOI: 10.13841/j.cnki.jxsj.2020.s2.047

[13] Wu Haibo, Xing Peng, Zhou Jiangbin. Theoretical study and test validation on vehicle rearview mirror whistling based on γ corrected transition model [J]. Automotive engineering, 2021, 6(43): 885-890. DOI: 10.19562/j.chinasae.qcgc.2021.06.012

[14] Wu Haibo, Xing Peng, Zhou Jiangbin. Theoretical study and test validation on vehicle rearview mirror whistling based on γ corrected transition model [J]. Automotive engineering, 2021, 6(43): 885-890.

[15] He Yingzhi, Yang Zhigang, Wang Yigang. The Mechanism and Experimental Study of the Effects of Car Body Sealings on Interior Aerodynamic Noise [J]. Automotive engineering, 2012, 8(34): 692-695. DOI: 10.3969/j.issn.1000-680X.2012.08.006

[16] Tao Zhi, Ma Yao, You Ruquan et al. A review of the research progress of boundary layer theory [J]. Scientia sinica technologica, 2024, 6(54): 979-1002. DOI: 10.1360/SST-2023-0316

[17] Zhang Feng, Cao Wei, Zhou Heng. Study of the Mechanism of Breakdown in Laminar-Turbulent Transition of a Supersonic Boundary Layer on a Flat Plate [J]. Applied Mathematics and Mechanics, 2006, 27(4): 379-386.

[18] Lounsberry T, Gleason M, Puskarz M. Laminar flow whistle on a vehicle side mirror [C]. America: Detroit, SAE Technical Papers, 2007. DOI: https://doi.org/10.4271/2007- 01-1549